https://doi.org/10.5194/os-2019-60
Preprint. Discussion started: 31 July 2019

Ocean Science
Discussions
Open Access
EGU

Surface waters properties in the Laptev and the East-Siberian Seas in summer 2018 from in situ and satellite data

Anastasiia Tarasenko[1, 2], Alexandre Supply[3], Nikita Kusse-Tiuz[1], Vladimir Ivanov[1], Mikhail Makhotin[1], Jean Tournadre[2], Bertrand Chapron[2], Jacqueline Boutin[3], and Nicolas Kolodziejczyk[2]

[1]Arctic and Antarctic Research Institute, Saint-Petersburg, Russia
[2]Univ. Brest, CNRS, IRD, Ifremer, Laboratoire d'Océanographie Physique et Spatiale (LOPS), IUEM, Brest 29280, France
[3]Sorbonne Université, CNRS, IRD, MNHN, Laboratoire d'Océanographie et du Climat, Expérimentations et Approches Numériques (LOCEAN), Paris, France

Correspondence: Anastasiia Tarasenko (tad.ocean@gmail.com)

Abstract. Variability of surface water masses of the Laptev and the East-Siberian seas in August-September 2018 is studied using in situ and satellite data. In situ data was collected during ARKTIKA-2018 expedition and then completed with satellite estimates of sea surface temperature (SST) and salinity (SSS), sea surface height, satellite-derived wind speeds and sea ice concentrations. Derivation of SSS is still challenging in high latitude regions, and the quality of Soil Moisture and Ocean Salinity (SMOS) SSS retrieval was improved by applying a threshold on SSS weekly error. The validity of SST and SSS products is demonstrated using ARKTIKA-2018 continuous thermosalinograph measurements and CTD casts. The surface gradients and mixing of river and sea waters in the free of ice and ice covered areas is described with a special attention to the marginal ice zone. The Ekman transport was calculated to better understand the pathway of surface water displacement. T-S diagram using surface satellite estimates shows a possibility to investigate the surface water masses transformation in detail.

1 Introduction

The eastern part of the Eurasian Arctic remains one of the understudied areas of the Arctic Ocean. The recent ARKTIKA-2018 expedition combined with novel satellite sea surface salinity and other parameters provide an unprecedented documentation of the temporal evolution of the surface water properties in the Laptev and East-Siberian Seas in summer 2018. The Laptev sea is shallow in its southern and central part (50-100 m) with a very deep opening on the north (3000 m). Several water masses are mixing there. The Lena and the Khatanga rivers discharge fresh water in the shallowest part of the Laptev sea on the south, the Kara sea water enters via the Vilkitskiy and Shokalskiy straits, the Atlantic water (AW) arrives along the continental slope to the north of the Severnaya Zemlya archipelago and further eastward, the Arctic water exists in the northern part (Rudels et al. (2004), Janout et al. (2017), Pnyushkov et al. (2015)). In the Arctic region, a strong seasonal warming and cooling, sea ice melting and freezing modify temperature and salinity in the upper layer, and therefore, complexify the vertical structure of

https://doi.org/10.5194/os-2019-60
Preprint. Discussion started: 31 July 2019

water column creating fronts at sea surface and "modified layers" in the interior (Rudels et al. (2004), Pfirman et al. (1994), Timmermans et al. (2012)). Dmitrenko et al. (2005) and Bauch and Cherniavskaia (2018) have shown that interannual changes of river discharge and wind patterns define the position of the oceanographic fronts in the central part of the Laptev Sea. To the best of our knowledge, no study has shown yet the evolution of the water masses on a synoptic scale in this region. In this study, we propose to follow the upper ocean waters displacement and its causes on a daily basis.

The most common concept of the upper ocean layer is a "mixed layer depth" (MLD) concept: between the ocean surface being in contact with the atmosphere and a certain depth, temperature and salinity are homogeneous. It is defined via a certain vertical gradient in density and/or temperature (de Boyer Montégut et al. (2004), Timokhov and Chernyavskaya (2009)), the maximum of Brunt-Väisälä frequency (Vivier et al. (2016)), or via the energy vertical distribution (Tryoshnikov (1979)). For the Arctic, the reported mixed layer depth varies between 5-7 m and 30-50 m depending on a region: open water or under the ice, the Barents Sea, the East-Siberian Sea or the central Arctic (Castro et al. (2017), Vivier et al. (2016), Pfirman et al. (1994), Timokhov and Chernyavskaya (2009)).

At the same time, the study of Timmermans et al. (2012) proposes to use for the Arctic ocean a term "surface layer" instead of the "mixed layer", because the water horizon lying between the sea surface and the Arctic main halocline can be weakly stratified even though the halocline hampers an active exchange of matter and energy. The main halocline is situated at 50-100 m in the Eastern Arctic (Dmitrenko et al. (2012)), 100-200 m in the Western Arctic ocean (Timmermans et al. (2012)). Using the concept of "surface layer" with some assumptions, the processes above the mentioned depths can be discussed separately from the interior.

The position of the pycnocline in the Arctic is mostly defined by the salinity. One of the first studies of Aagaard and Carmack (1989) devoted to the freshwater content was using 34.80 PSS as a reference salinity value separating the "fresh" and the "saline" waters, as at that moment it was a mean Arctic salinity. This value is used as well in more recent overviews (Haine et al. (2015)). In the study of Rabe et al. (2011) a depth of 34 PSS isohaline was used to estimate the liquid freshwater content in the Arctic ocean. Cherniavskaia et al. (2018) based on in situ data in the Laptev sea for 1950-1993 and 2007-2012 periods reported the overall salinity in the surface 5-50 m layer to lie within a range from 30.8 to 33 PSS. Between the very surface layer and the Atlantic waters, Dmitrenko et al. (2012) finds modified "lower halocline" waters with typical characteristics of salinity (between 33 and 34.2 PSS) and negative temperatures (below -1.5°C); in 2002-2009 this layer was situated at 50-110 m depths.

A general study of Polyakov et al. (2008) on the Arctic ocean freshening defines the upper ocean layer between 0 m and a depth of a density layer $\sigma_\theta = 27.35$. This isopycnal is often located at 140–150 m, "slightly above the Atlantic water upper boundary defined by the 0°C isotherm".

To analyse the upper-ocean processes, we will focus on the very surface with satellite data and on the upper 250 m layer with the CTD casts, showing the isohaline and isopycnal positions. Such approach to the "upper layer" is necessary to know the upper limit of the Atlantic waters, though not being the subject of this study, but essential for the water mass transformation.

https://doi.org/10.5194/os-2019-60
Preprint. Discussion started: 31 July 2019

August and September are two summer months that are very important for heat exchange between the open ocean and atmosphere over the Laptev sea. In a recent study, Ivanov et al. (2019) reported that during this time period when the sea ice is melting the ocean is opening, a radiative balance changes from 100 W/m^2 to negative values, following the seasonal cycle of shortwave radiation. The sea level anomalies over the Eastern Arctic shallow seas are positive and largest in summer (up to 10 cm at 75°N, down to 3 cm at 80°N, as reported by Andersen and Johannessen (2017)). The Laptev sea considered in this article is not at all sampled by Argo products, so the ARKTIKA-2018 measurements offer a good opportunity to validate SST and SSS. Accurate measurements of surface salinity can enrich our understanding of freshwater content in the Arctic (Rabe et al. (2011)) and SSS estimates from L-band satellites can bring a valuable input.

In this paper, the surface water evolution of the Laptev and the East-Siberian seas will be described and analysed considering wind speed and direction during the period of the ARKTIKA-2018 expedition. Firstly, data and methods used for the following study will be presented. Then, we compare SST and SSS satellite estimates with in situ measurements. The influence of the wind speed on Laptev sea is discussed considering Ekman transport and pumping. Finally, the better understanding allows to describe the water masses of the Laptev sea and their transformation during August-September 2018.

2 Data and Methods

2.1 In situ measurements during the ARKTIKA-2018 expedition

Oceanographic measurements during the ARKTIKA-2018 cruise on board RV Akademik Tryoshnikov started on August 21, 2018 and ended on September 24, 2018 (Fig.1). Standard oceanographic stations (145 in total) were conducted with Sea-Bird SBE 911plus CTD instrument. Oceanographic sections were organized in the way to best represent the processes between the shallow and continental slope areas, but also in the straits between the Kara and the Laptev sea: Vilkitskiy Strait southward to the Bolshevik Island, with depths from 70 to 1500 and the narrow and rather shallow (250 m) Shokalskiy Strait between the Bolshevik and the October Revolution Islands. Part of the measurements were carried out in marginal ice zone (MIZ) and ice-covered area. In this study we define MIZ as an area with 0-30% sea ice concentration close to the ice edge.

The ship was equipped with an underway measurement system Aqualine Ferrybox, widely known as thermosalinograph, TSG. The instrument had a temperature and a conductivity (MiniPack CTG, CTD-F) sensors and a CTG UniLux fluorometer installed; thus, continuous temperature, salinity and chlorophyll-a estimations were obtained along the ship's trajectory. The inflow is situated at 6.5 m below the surface (the inflow hole is on the ship's hull). All data were processed and filtered for random noise and bad quality data, and then compared and calibrated with CTD measurements. The cruise data can be found at https://uaf-iarc.org/nabos/.

2.2 Satellite data

Satellite data provide an instant information about surface distribution of geophysical characteristics over the whole study area and their temporal evolution.

https://doi.org/10.5194/os-2019-60
Preprint. Discussion started: 31 July 2019

Ocean Science
Discussions
Open Access
EGU

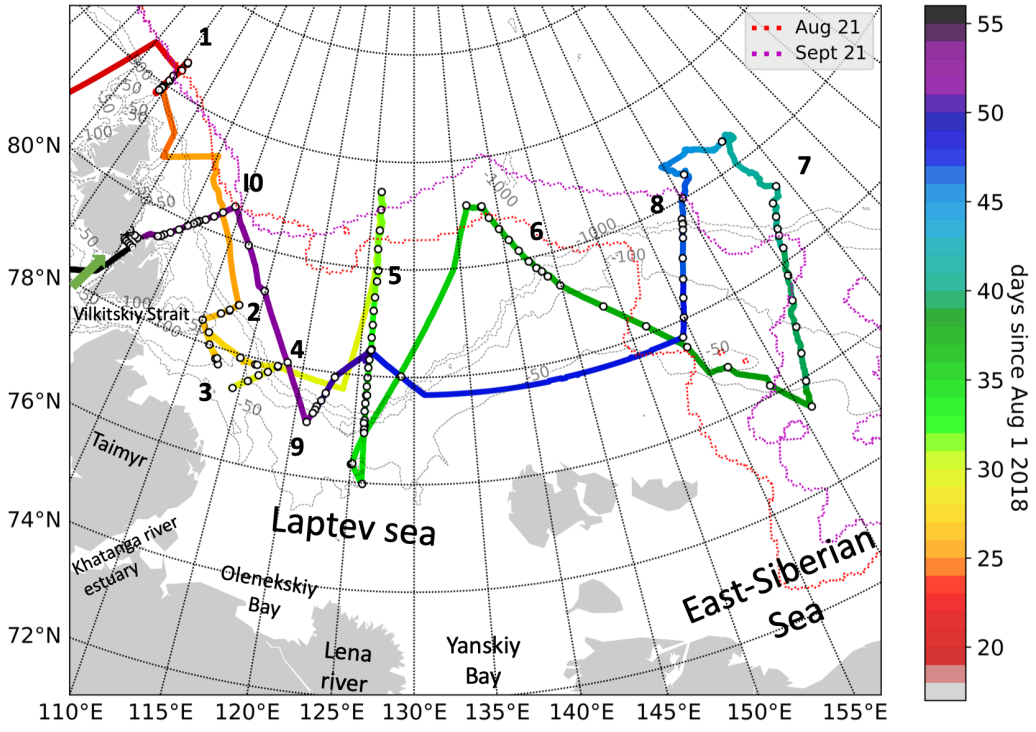

Figure 1. Time of the ARKTIKA-2018 expedition works and bathymetry from ETOPO1 "1 Arc-Minute Global Relief Model" (Amante and Eakins (2009)). CTD stations are shown with white squares. Color bar indicates the number of days since August 1, 2018. The sea ice edge positions are indicated with a dashed lines for the beginning (August 21) and the end of expedition (September 21). The numbers indicate 10 transects that will be studied later in the paper. The green arrow indicates the Shokalskiy Strait.

All listed below products were considered from August 1, 2018 to September 25, 2018 (the last day of ARKTIKA-2018 expedition). If not indicated additionally, for consistency all products were interpolated on a regular grid within the bounding box 74-85N 90-170E, with 0.01 degree step in latitude, and 0.05 degree in longitude. The spatial resolution of selected grid roughly corresponds to 1 km on the studied latitudes.

2.2.1 Sea surface temperature

The SST-retrieving instruments with the highest resolution, such as AVHRR, MODIS and VIIRS work in Near Infrared (NIR) and Infrared (IR) bands and depend strongly on atmospheric conditions (provide measurements for clear sky). For lower resolution microwave instruments, such as AMSR2, the clouds are not opaque, but SST retrieval may still be hampered by high wind speed and precipitation events. As satellite measurements in IR and NIR ranges are sparse because of the frequent cloudiness over the Arctic ocean, a use of a blended product can be favorable. In this paper we use the Danish Meteorological Institute Arctic Sea and Ice Surface Temperature (hereafter referred as "SST DMI"). SST DMI is a Level 4 daily product

https://doi.org/10.5194/os-2019-60
Preprint. Discussion started: 31 July 2019

provided by the Copernicus Marine service. Daily surface temperatures over the sea and ice are calculated on a 5 km spatial grid from several instruments: AVHRR and VIIRS for SST and AMSR2 for sea ice concentration, using optimal interpolation (Høyer et al. (2014)).

2.2.2 Sea surface salinity

Soil Moisture and Ocean Salinity (SMOS) was the first satellite mission embarking an L-band microwave radiometer, which measurements make possible to derive sea surface salinity (SSS). With recent processing, the standard deviation of the differences between 18-day SMOS SSS and 100-km averaged ship SSS is 0.20 PSS in the open ocean between 45°N and 45°S (Boutin et al. (2018)). However, the precision degrades in cold water as the sensitivity of L-band radiometer signal to SSS decreases when SST decreases, even though this effect on temporally averaged maps is partly compensated by the increased number of satellite measurements at high latitude. A possibility of using SSS estimates in cold regions derived from L-Band radiometry was, however, demonstrated recently by several working groups (Tang et al. (2018), Grodsky et al. (2018), Olmedo et al. (2018)). However SMAP CAP/JPL or SMOS BEC L3 products are spatially averaged from 60 km to more than 100 km. Soil Moisture Active and Passive (SMAP) L3 SSS v3 from REMSS provides a 40km resolution version but do not provide a sufficient coverage in the Laptev Sea. The methodology developed in this study for retrieve SMOS weekly SSS aims at maintaining SMOS SSS original spatial resolution and at attempting to retrieve SSS as close as possible to the ice edge.

Weekly SSS average investigated in this study are computed using SMOS SSS L2 from the ESA last processing (v662, Arias and Laboratories (2017)). L2 SSS are available on the ESA SMOS Online Dissemination website. The mean spatial resolution of individual SMOS SSS is close to 50 km. SMOS SSS products are sampled over an Icosahedral Snyder Equal Area (ISEA) grid at 15 km resolution. Seven days running means are computed each day in each pixel. SSS are temporally weighted using a Gaussian function with a standard deviation of 3 days. The full width of SMOS ascending and descending orbits swaths is considered in order to take advantage of better temporal and spatial sampling over the Arctic ocean and decrease the uncertainty with temporal averaging. In order to eliminate SSS at very low and high wind speeds because of their high uncertainties, SMOS SSS are considered only if the associated ECMWF wind speeds are between 3 and 12 m/s. SSS measurements are also weighted by the estimated error of the SSS measurement (as in (Yin et al. (2013), equation A7). This error is derived from the SSS theoretical error multiplied by the normalized χ^2 cost function. Dinnat et al. (2019) have shown that the Klein and Swift (1977) dielectric constant model is inaccurate at low SST. In order to mitigate this effect, a SST-dependent correction derived from the Fig. 16 of Dinnat et al. (2019) (blue-circle line) has been applied. Finally, a criterion on SMOS-retrieved pseudo-dielectric constant (ACARD parameter) is applied to discard SMOS measurements affected by sea ice. The error on the weekly SSS mean is derived from the propagation of the error on individual SSS. It increases strongly in the vicinity of sea ice. For this reason, in the following study, above 75°N, all pixels with a SSS weekly error larger that 0.8 PSS are not considered. South of 75°N, a higher threshold is used (1.5 PSS) allowing to maintain some measurements close to the source of the river plume. In this area, the χ^2 may increase due to the strong heterogeneity of SSS within SMOS multi-angular brightness temperatures footprints, and the number of measurements is low due to the combined presence of the coast and islands but without ice sheet.

https://doi.org/10.5194/os-2019-60
Preprint. Discussion started: 31 July 2019

2.2.3 Sea ice concentration and ice masks

Sea ice masks were obtained from AMSR2 sea ice concentrations products provided by the University of Bremen (Spreen et al. (2008)): they are weather-independent, thus, continuous for all time period. The highest available spatial resolution is 3.125 km. The AMSR2 ice masks were used in addition to the masks provided with every satellite product discussed. A continuous erroneous presence of ice along the Siberian coast was observed and had to be filtered: images in optical band and the ice charts from the Arctic and Antarctic Research Institute (AARI) were used as a reference. As detailed in section 2.2.2, additional filterings were applied to SMOS SSS as L-Band measurements are sensitive to ice thicknesses less than 50 cm contrary to AMSR2 measurements.

2.2.4 Wind speed

To investigate the winds speed patterns, we used ASCAT scatterometer daily C-2015 L3 data produced by Remote Sensing Systems. Data are available at www.remss.com.

2.3 Reanalysis data

Reanalysis data were used to include some additional parameters not available from satellite and in situ data. Atmospheric forcing fields - sea level pressure, SLP, and air temperature, were obtained from the ERA5 reanalysis (Bertino et al. (2008)). The latest reanalysis of ERA5 still have relatively crude spatial grid of 0.5°for the SLP and 0.25°for air temperature.

3 Results

3.1 Comparison of datasets

To illustrate the consistency of the different satellite products, September 13, 2018 was considered as it is one of the rare days in summer 2018 when the central part of the Laptev sea was cloud-free, which is especially important for SST.

3.1.1 Temperature

The SST field from DMI L4 product for September 13, presented in Figure 2 shows a rather complex pattern with a pronounced gradient associated with river waters in the central part of the Laptev sea. Besides the full coverage over the studied area, the advantage of blended DMI product is that it takes into account ice temperatures, so the Marginal Ice Zone (MIZ) is better represented and not masked out. The total number of SST measurements ingested by SST DMI L4 over the studied area from August 1 to September 25, 2018 varies from 1000 to 2500 measurements per 1 pixel over the whole studied period. The error in temperature estimates provided by DMI, is shown in Fig.2. The highest potential error (up to 2.5°C), though observed over some open sea areas (due to potential cloudiness), is mostly associated with the sea ice due to its heterogeneity. Over most of the southern and the central part of the free-of-ice Laptev and the East-Siberian seas, the error is below 0.5°C and over the eastern part, it is below 1°C for selected day.

https://doi.org/10.5194/os-2019-60
Preprint. Discussion started: 31 July 2019

The first step of satellite and in situ dataset evaluation was a value-by-value comparison of collocated dataset (nearest neighbor) and calculation of basic statistics. For this analysis, we collocated satellite-estimated temperature with the in situ measurements in the upper 6.5 m layer: CTD averaged every half a metre above 6.5 m depth and TSG at 6.5 m depth averaged every 30 minutes. The median depth of the collocated temperature measurements is 5.25 m due to the absence of CTD data in the very first metres. As the ship was moving with an average (median) speed of 8 knots, 30 minutes averaged TSG's temperature corresponds to the median of measured temperature over approximately 7.5 km, which is comparable with the spatial resolution of DMI SST L4 10 km. There were 1707 points in the analysis.

Though, in fact, satellite sea surface temperature estimates may differ from the measurements at 6.5 m, we expect some general consistency between the datasets. Studies carried out by Castro et al. (2017), devoted to the validation of MODIS SST in the MIZ, and that by Vivier et al. (2016) which describes in situ measurements in iced-covered area, report that the first 7-10 m layer below the surface is mostly homogeneous. Nevertheless, diurnal warming and local vertical mixing can affect the temperature distribution in the very surface layer. Local diurnal variations of temperature are supposed to be filtered out in the blended DMI product, as it only uses observations between 21:00 and 7:00 local time (Høyer et al. (2014)), but can still be present in real in-situ measurements.

Comparison of the DMI SST and in situ surface-layer temperature (Fig. 2) shows a very good agreement almost independent on area and time during ARKTIKA-2018 expedition. The correlation coefficient is 0.89, and the RMS is 0.77°C. The bias between mean in situ and mean DMI SST data is -0.19°C, where the DMI-SST is higher than the in situ temperature. This value seems to be realistic, because according to CTD and TSG measurements, in average, the 0-3 m water layer is by 0.3 degree warmer than the 3-6.5 m layer. The largest deviations were observed when the expedition was working in the MIZ or compact sea ice, so they might be associated with either imperfect sea ice flagging of some stages of sea ice in the blended DMI "SST and sea ice temperature" product, or an introduced noise after re-interpolation of data on a regular grid. This noise together with the different sampling of SST by in situ and DMI L4 product lead to a standard deviation of the difference between in situ and DMI SST larger than the error provided in the DMI product (Fig. 2, lower right). Overall, DMI L4 blended SST agrees well with in situ data, so we use this product for the following analysis of SST time-series.

3.1.2 Salinity

In this section, we compare SMOS SSS relative to in situ measurements. Figure 3 presents the SMOS SSS. We carry a collocation of SSS and in situ measurements of salinity in the upper 6.5 m layer, similar to that one for the temperature described above, except that the averaging of the TSG salinity was done over one hour period (equal to ~ 15 km distance) in order to be closer to SMOS resolution. Comparison between SMOS retrieved error and error based on comparison with cruise salinity measurements is presented in Fig. 3. It shows a good agreement between distribution of SMOS SSS weekly error estimated from retrieval process and distribution of error obtained from comparison with Akademik Tryoshnikov salinity measurements. This results allow us to use SMOS error with a higher confidence in our further analysis. Take into account the SMOS error makes possible to increase the quality of the comparison between the SMOS SSS and the vessel SSS. Using error filtering, points too close to the ice edge are excluded. We used 985 collocated points. Comparison between the in situ salinity and

https://doi.org/10.5194/os-2019-60
Preprint. Discussion started: 31 July 2019

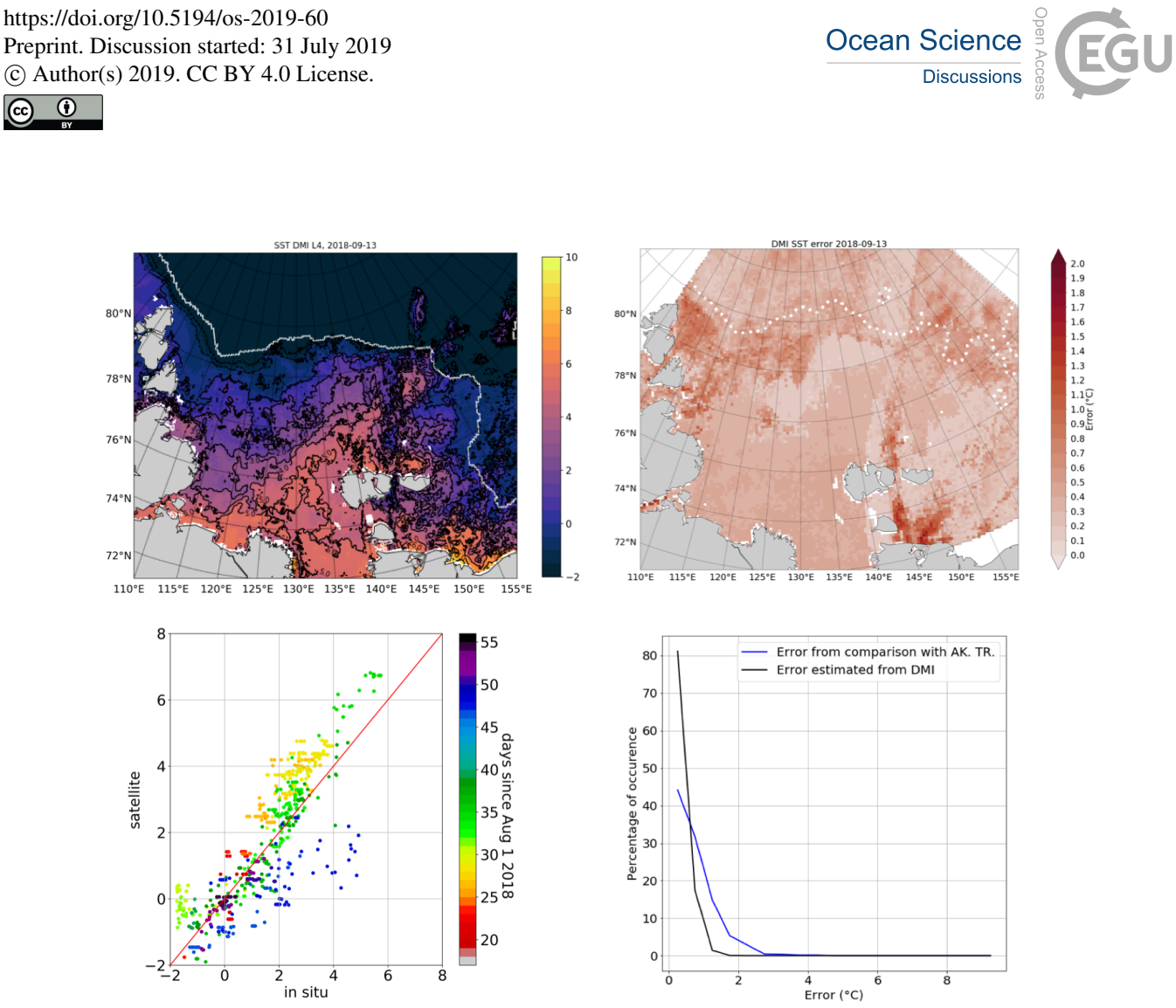

Figure 2. Sea surface temperature validation: example of DMI SST L4 image for September 13 (upper left) with the provided error estimates (upper right); comparison of collocated SST and in situ data (CTD and TSG) in the upper 6.5 m (lower left) and distribution of error provided by DMI and absolute difference measured from comparison with in situ data (lower right). The percentage of occurrence is computed in temperatures classes with a size of 0.5 degrees that starts at 0 degrees.

SMOS post-processed SSS shows a very good agreement, not yet demonstrated before by any other salinity product in the Laptev sea. The correlation coefficient is 0.86 with a RMS = 0.86 PSS. The bias is 2.06 PSS. For the further analysis we subtracted this bias from the entire SMOS SSS dataset. Standard deviation of SMOS SSS with respect to in situ SSS do not depend on the depth of in situ salinity measurements above 6.5 m, either because in situ salinity is homogeneous vertically or because comparisons are too noisy to detect this small variations (not shown). Although SMOS shows a good agreement most of the time, some larger error can occur close to the ice margin or when pixels are contaminated by small ice pattern that are not detected by AMSR2 sea ice concentration (as at 125°E, 80°N in Fig. 3, top left).

https://doi.org/10.5194/os-2019-60
Preprint. Discussion started: 31 July 2019

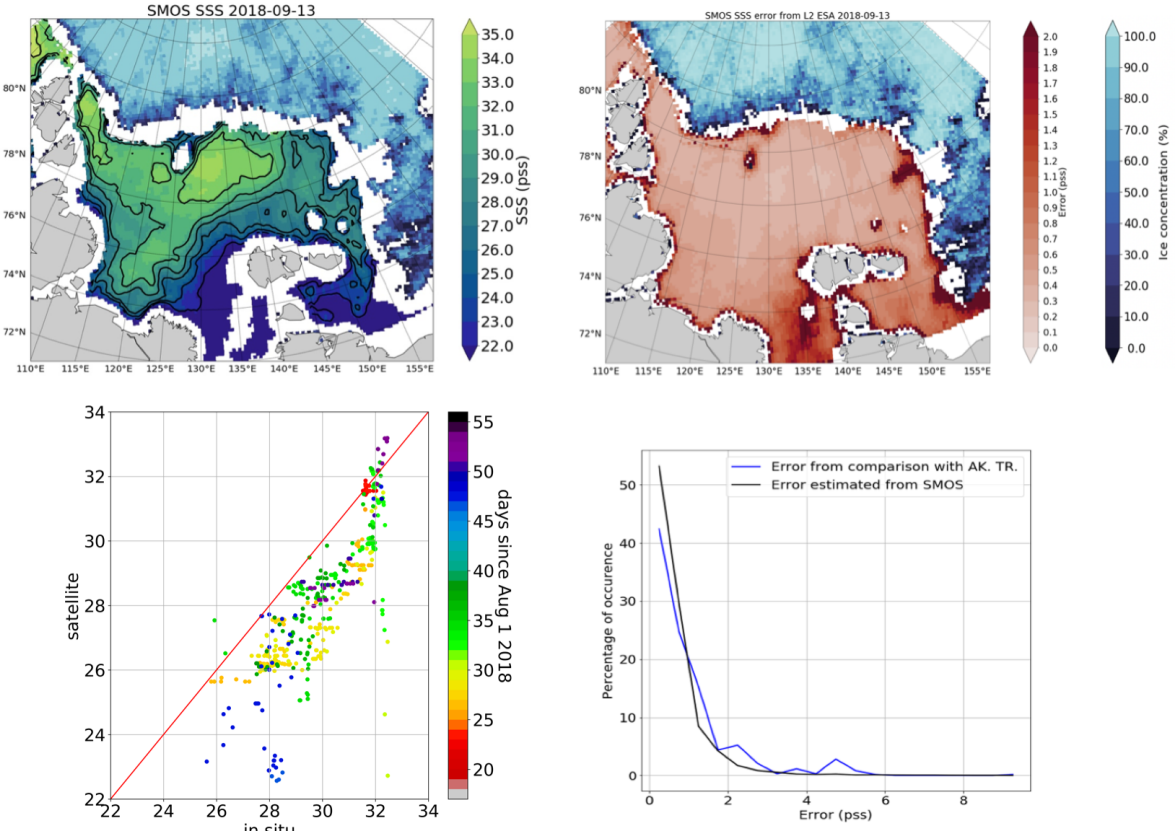

Figure 3. Sea surface salinity validation: example of SMOS SSS for September 13, 2018 (upper left), computed error estimates (upper right), comparison of collocated SSS and in situ data in the upper 6.5 m (lower left) and distribution of provided SMOS L2 error and measured absolute difference from comparison with in situ data (lower right). The percentage of occurrence is computed in salinity classes with a size of 0.5 pss that starts at 0 pss. Sea ice concentration from AMSR2 is indicated with blue colors

4 Overview of SST and SSS in the Laptev and East-Siberian seas in summer 2018

The mean SST during 2 summer months is 2.181°C in the Laptev sea (between Severnaya Zemlya archipelago and New Siberian Islands), and 1.126 °C in the studied part of the East-Siberian sea (Fig. 4). The highest temperatures (above 6°C) were observed close to the Lena river delta in the Yanskiy Bay and in the Olenekskiy Bay in front of the Khatanga river. A warm water pool associated with the river plume between 125°E and 135 °E progressively propagates northeast and warms up this part of the sea: 0°C isotherm at 140°E meridian is situated 100 km northward compared to its position at 120°E. The studied part of the East-Siberian sea was not completely free of ice in August-September 2018. Negative temperatures are observed near the ice edge at a distance of 50-100 km almost everywhere, except for a small area at 80°N 160°E, where warm river water meets the sea ice and no open water with negative temperatures is seen. The strongest gradients are observed along the sea ice edge and the river waters plume (up to 0.05° C/km). Standard deviation in Fig.4 is the largest in the Olenekskiy

https://doi.org/10.5194/os-2019-60
Preprint. Discussion started: 31 July 2019

Bay (over 2.5°C), along the coastline close to the Lena river delta (about 4°C) and in marginal ice zone (mostly over 1.5°C). The remarkable variation of temperature in the central part of the Laptev sea should be associated with the thermal fronts displacement.

The averaged SSS is 28.75 PSS in the Laptev sea and 27.74 PSS in the studied part of the East-Siberian sea (Fig. 4). The spatial distribution of mean salinity for August-September 2018 has several characteristic features. The freshest waters (below 20 PSS) are observed within the river plume northeast of the Lena river delta and within the southern part of the East-Siberian sea. Fresh waters with salinity below 28 PSS reach the sea ice edge in the northeast Laptev sea. Additional freshwater from the Kara sea enters via the Vilkitskiy and Shokalskiy straits in the west (28-30 PSS) and is also observed along the sea ice edge, so it could be associated with ice melting. The most saline waters (above 34 PSS) are situated in the central part of the Laptev sea near 78-80°N 120-140°E, and in the northwest, along the Severnaya Zemlya Archipelago. As also observed in the SST, the SSS in the Olenekskiy Bay is highly variable, which can be explained by the variation of the freshwater discharge during the 2 months. Nevertheless, large SSS variability is also observed all along the sea ice edge: at 78-80°N in the north and northwest and at the boundary between the Laptev and East-Siberian seas. This large variability can be explained in two ways: physical (natural haline fronts related to sea ice melting) and instrumental (remaining ice contaminated pixels, lower sensibility of L-band in cold waters). At 125°E, free-floating patches of broken ice detached from compact sea ice edge were observed during several weeks in August-September 2018. Random pieces of broken ice are not always recognized by ice-mask filters, so can artificially increase the SSS variability. At the same time, this is the area where river waters meet sea ice, which induces natural variability.

4.1 Freshwater plume extension

To evaluate the distribution of freshwater input in the Laptev sea during summer months, we considered zonal and meridional transects along 78°N and 126°E, respectively and plotted their temporal evolution on Hovmöller diagrams (Fig. 5, 7).

The zonal transect helps to investigate the mean stream position of the river plume away from the coast, in the central part of the Laptev sea with more complex topography. In the western part (up to 130 °E), the transect is located roughly above the continental slope and then over the shelf (Fig.5). It can be noticed that a displacement of river waters roughly follows that of sea ice edge on the east and is bounded by the edge of the shelf on the west. Overall, temperatures are higher in August than in September: a warm pool with SST over 6 °C is observed during the first 30 days at 78°N, 130-147 °E, with highest temperatures on August 26. These coordinates define the position of the river plume at 78°N latitude, as it can be clearly seen in the salinity values varying from 27-30 PSS there. Relatively strong daily winds (10-12 m/s) observed during the first 10 days of September are associated with a passage of series of cyclones and strongly impact the surface layer: the median temperature over the zonal transect decreases from 3°C to almost 0°C, and salinity changes by 1 PSS. As the amount of incoming solar radiation diminishes in September, the maximum SST values do not exceed 3°C anymore. Nevertheless, in the end of September a new freshwater patch is seen at 140°E (less observed in SST field) indicating that the surface mixed layer "upstream" (in the southern part of the Laptev sea) contains sufficient amount of freshwater to restore its previous state after a mixing event.

https://doi.org/10.5194/os-2019-60
Preprint. Discussion started: 31 July 2019

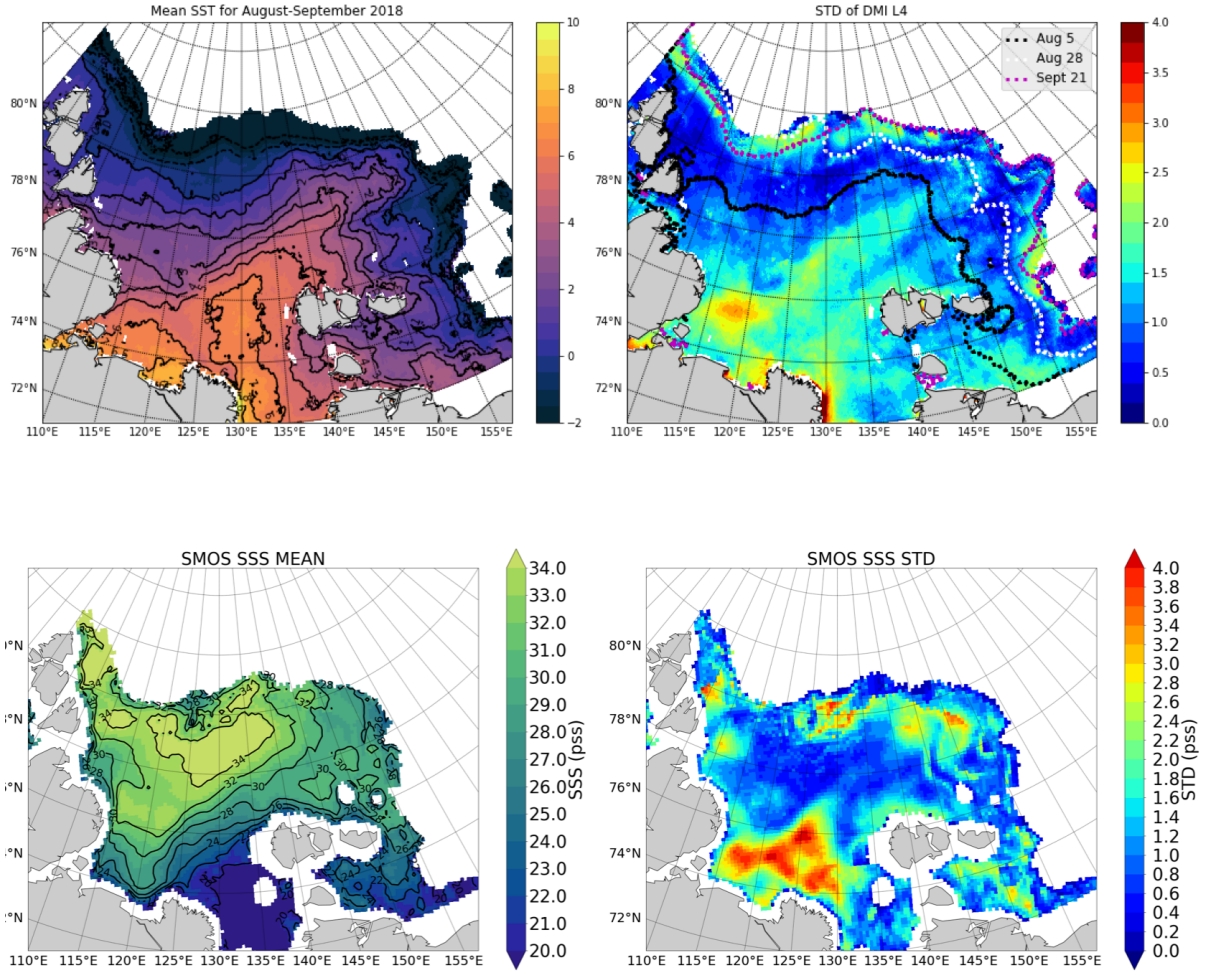

Figure 4. Mean DMI SST (upper row) and SMOS SSS (lower row) with their standard deviation for August-September 2018

4.1.1 Kara sea waters

Zonal transect allows to see not only the Lena river plume, but to observe as well the Kara water intrusions on the West. Selected zonal transect at 78°N is partly lying above the Vilkitskiy Strait connecting the Kara and the Laptev seas. In salinity fields of the zonal Hovmöller diagram, we observe the freshwater arriving from the Kara sea at 110-115°E with typical values of 25-28 PSS during the first 20 days of August and in the end of September. It is remarkable, that SST fields do not indicate the presence of these intrusions so clearly. It might be possible, that fresh waters of the Ob' and Yenisei rivers arriving to the Laptev sea have already lost a significant part of their heat content via exchange with the atmosphere, but the fresh water layer wasn't completely mixed with surrounding sea environment. In Fig. 6, the CTD data justify that the amount of fresh water arriving

https://doi.org/10.5194/os-2019-60
Preprint. Discussion started: 31 July 2019

Ocean Science
Discussions
Open Access
EGU

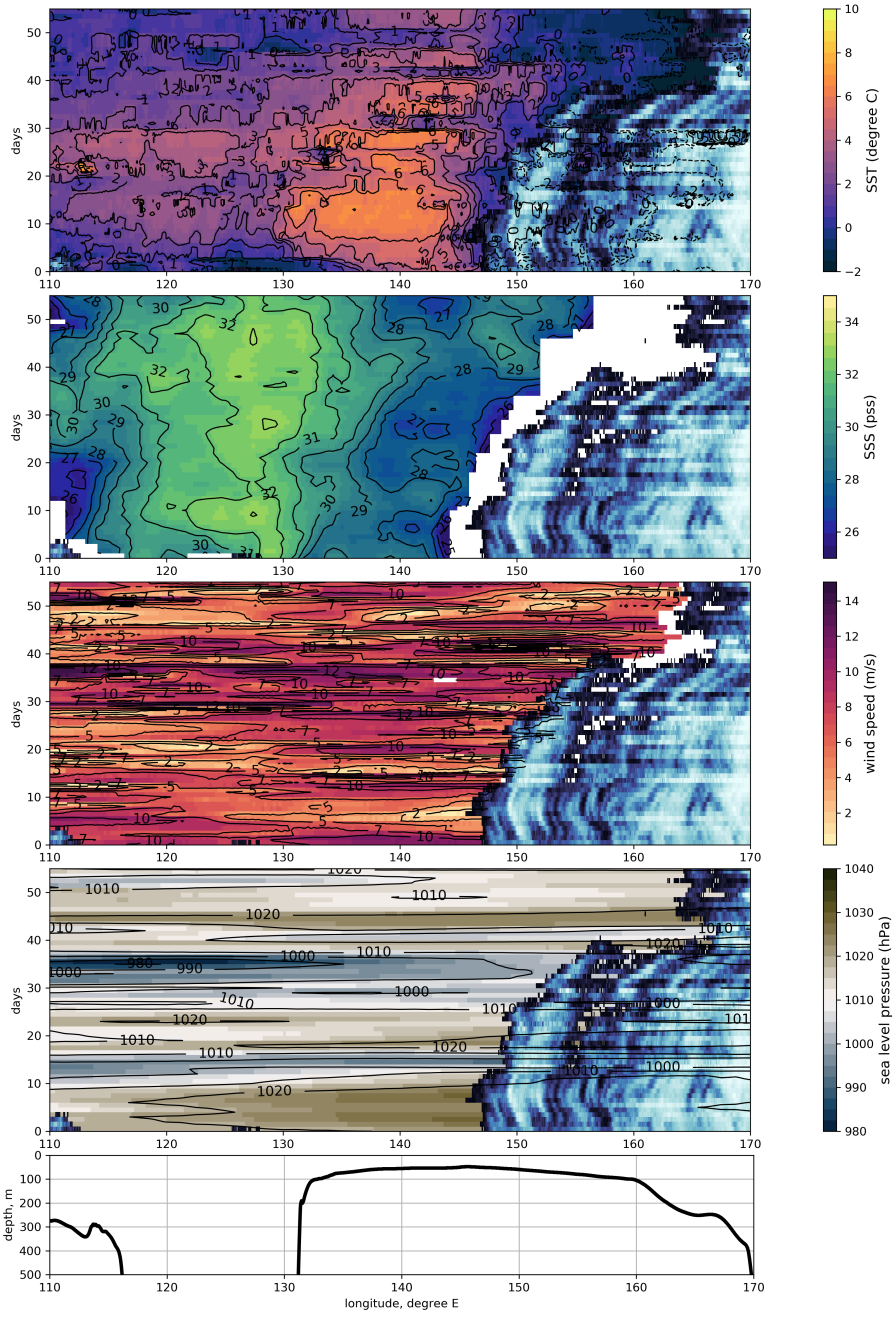

Figure 5. Hovmöller diagram of SST, SSS, wind speed, and sea level pressure for the zonal transect at 78°N. Sea ice concentration is indicated with a blue color, see Fig.3

https://doi.org/10.5194/os-2019-60
Preprint. Discussion started: 31 July 2019

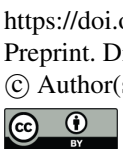

Ocean Science
Discussions
Open Access
EGU

from the Kara sea via Vilkitskiy strait is significantly greater than freshwater arriving via the narrow and rather shallow (250 m) Shokalskiy Strait between the Bolshevik and the October Revolution Islands or north of the Severnaya Zemlya archipelago at the traverse of the Arkticheskiy Cape across the continental slope. The temperature of the surface layer is increasing from the North to the South from 0°C to 3.5 °C. The salinity sections indicate the freshwaters with salinity above 29 PSS only in the Shokalskiy and the Vilkitskiy straits, which suggests very little advection of the Kara-origin fresh waters via the north. From the buoyancy cross-sections, one can find that the strongest stratification is at 5-20 m depth, which corresponds to the 1024-1025 kg/m^3 isopycnals position. This result argues a definition of fresh-water content by the 1027.35 kg/m^3 isopycnal of Polyakov et al. (2008), as the surface salinity and temperature in the Siberian shelf seas are lower than in other regions. The definition of fresh water content in the Arctic might be considered again.

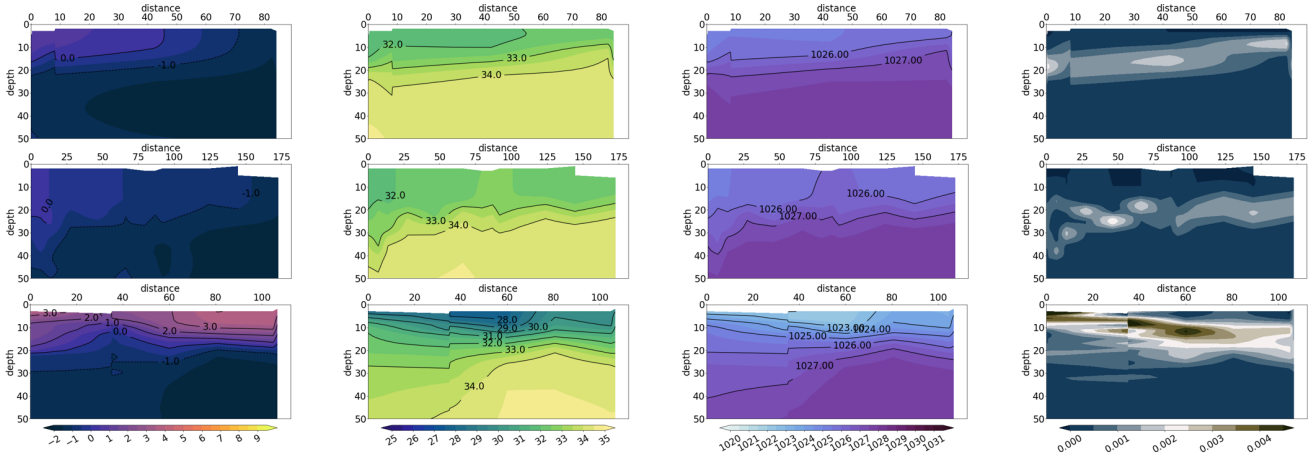

Figure 6. Temperature, °C, (left, first column), salinity, PSS, (second column), water density, kg/m^3 (third column) and buoyancy frequency, $1/s$, (right, forth column) obtained from CTD measurements in the upper 50 m for section 1 northward of Arkticheskiy Cape (upper row), section 10 across the Shokalskiy Strait (second row), and section 4 across the Vilkitskiy Strait (lower row). See Fig.1 for the section's positions. The zero km is always placed at the southern point of each section

The meridional transect along 126°E (Fig. 7) partly corresponds to the standard oceanographic section 5 carried out during ARKTIKA-2018 expedition on September 1-4, 2018 (Fig.8). This transect helps to understand the northward propagation of the river plume and to evaluate the freshwater content using in situ data. The highest temperature observed at this longitude is 8°C in August (please note, that small cold temperature intrusion days 22-26 most likely corresponds to the error in DMI L4 product due to a cyclone passage, which is seen on when comparing DMI to AMSR2 microwave data (not shown here)).

The warmest and freshest waters of river plume occupy the area between 74-77°N in August and progressively retreat in September: SST and SSS gradients become wider and less pronounced, temperature decreases to 3-4 degrees. High winds speed (10-12 m/s) associated with a depression passage during the first two weeks of September are seen both on the meridional and the zonal Hövmoller diagrams and might be related to this widening of the frontal area. Nevertheless, a cross-correlation between the time-series of wind speed and temperature or wind speed and salinity in a point with random coordinates does not

https://doi.org/10.5194/os-2019-60
Preprint. Discussion started: 31 July 2019

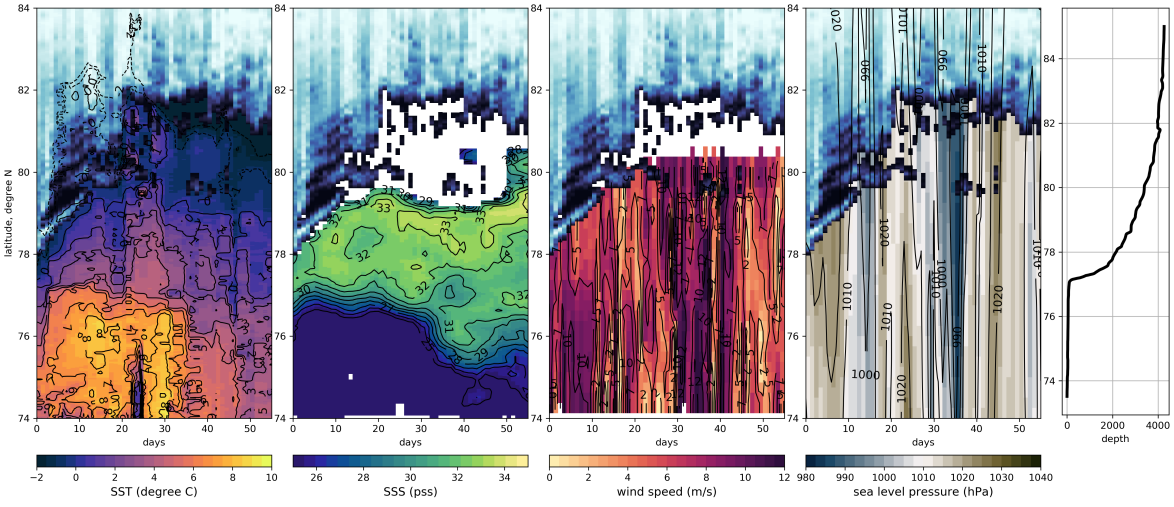

Figure 7. Hovmöller diagram of SST, SSS, and wind speed for the meridional transect at 126°E. Sea ice concentration is indicated with blue color, see Fig.3

give statistically significant results: both correlation coefficients are below 0.2 with any time lag (0-10 days). Better correlation is observed with sea level pressure (up to 0.6 at some points), but over the 56 days of the studied period it is not statistically representative as only two passages of cyclone were observed. Higher values of cross-correlation coefficient are expected over the frontal zone, as this is the area exposed to rapid changes.

Oceanographic sections allow to estimate a thickness of the freshwater layer and how far the river water propagates under the ice. Section 5 provides complementary information to the meridional Hovmöller diagram (Fig.8, upper row) as it was done along the same 126°E parallel from 76 to 81.4° N on September 1-4 2018. This moment corresponds to the passage of several cyclones over the Laptev sea, which, in turn, displaced the river front to the south, unfortunately, almost out of scope of this oceanographic section. Nevertheless, at 76-78° N (first 200 km of the section), low salinity between 29-33 PSS was still observed in the upper 25 metres. A thin upper layer with positive temperatures has the same thickness, but extends further northward, up to 79° N. In the north of the section, under the ice, the temperatures are below 0°C and salinity is rather low, below 32 PSS. The low salinity under the ice can indicate the residuals of the river waters arrived in this area earlier. If the river waters were propagating under the ice when the Laptev sea was not yet completely open, one should assume their further mixing with sea waters when the sea started to open in its central part (mixed waters with salinity between 30 and 32 PSS and still positive temperatures). The heat exchange with the sea ice might be more effective than with the atmosphere, so under the ice the temperatures are negative, and river water signal is not observed anymore, contrary to salinity.

Overall, the first 150 km over the shelf, where the warmest and freshest waters were observed, are characterized by the strongest stratification in the upper 25 m layer. This is the depth of a stable stratification for the whole section, though stratification is less pronounced in the deeper part of the sea than over the shelf. Below the pycnocline, one can observe cold (with

https://doi.org/10.5194/os-2019-60
Preprint. Discussion started: 31 July 2019

negative temperatures) and saline (salinity between 33 and 34.5 PSS) water mass. The warm and saline Atlantic water spreading along the continental shelf is best identified in temperature vertical profiles at 100-120 m depth, but is also detected by the instability signal (right column in Fig. 8). The propagation of the Atlantic waters is beyond the scope of this paper, and though Atlantic waters is observed in all presented below oceanographic sections, it won't be discussed furthermore.

When considering other meridional sections (section 6, 8, and 7 according to their positions from the west to the east), one can follow the eastward propagation of the river waters away from their origin, the Lena river delta. Section 6 started on September 5 in the vicinity of the marginal ice zone in the deep North-Eastern part of the Laptev sea and ended in the ice-covered part of the East-Siberian sea over the shelf on September 9. This section is not exactly perpendicular to the continental slope, so we can not estimate the width of the river waters plume, but overall the thickness of the upper layer is similar to that observed with section 5 in the deep part of the section (20-30 m). The waters over the shallowest part (depth smaller 60 m) were observed under the ice, which is clearly seen in temperature signal that is negative even close to the surface. At the same time, the main freshwater core with the highest temperature is observed above the shelf break. The second core is observed in the northern part of the section, with lower salinity than in the north of section 5. The mixing over the shelf was effective enough to stretch the isopycnals in the vertical up from the surface to the bottom. Nevertheless, the depth of the maximum stratification is close to 20 metres as for the shallow part of the section 5. Over the edge of the continental slope, the maximum Brünt-Väisälä frequency deepens to 25 m, and over the deep-water part to 30 m depth.

Section 8 was started on September 15 in MIZ over the deep part of the East-Siberian sea and finished by September 17 in the free-of-ice area over the shelf. The river signal is still very pronounced both in temperature and in salinity profiles, with an efficient mixing over the 60 m layer on the shelf and more condensed isopycnals over the shelf edge. The most eastern section 7 was conducted under the ice. The temperatures are, thus, negative above the Atlantic water, but salinity profile reveals the river water presence with freshwater core having salinity below 29 PSS. The maximum value of Brünt-Väisälä frequency are less than for other sections and are observed at 20 m depth and at 55 m depth, following 1024 kg/m^3 and 1026.5 kg/m^3 isopycnals, accordingly.

To resume, in the summer 2018, we observe a north-eastern displacement of the Lena river waters including in the MIZ and ice-covered area. We suggest that the active displacement started in the ice-covered conditions after the maximum of river discharge in July (following the Papa et al. (2008) study), then, with progressive opening, a part of the river waters was mixed within the upper layer of sea and exchanged the heat with the atmosphere. Regarding the waters under the ice, the heat flux from the river water to the sea ice resulted in cooling of these waters to the ambient negative temperature, but, at the same time, the sea ice protected the freshwater layer from wind-induced mixing, so it conserved a pronounced signal in salinity.

https://doi.org/10.5194/os-2019-60
Preprint. Discussion started: 31 July 2019

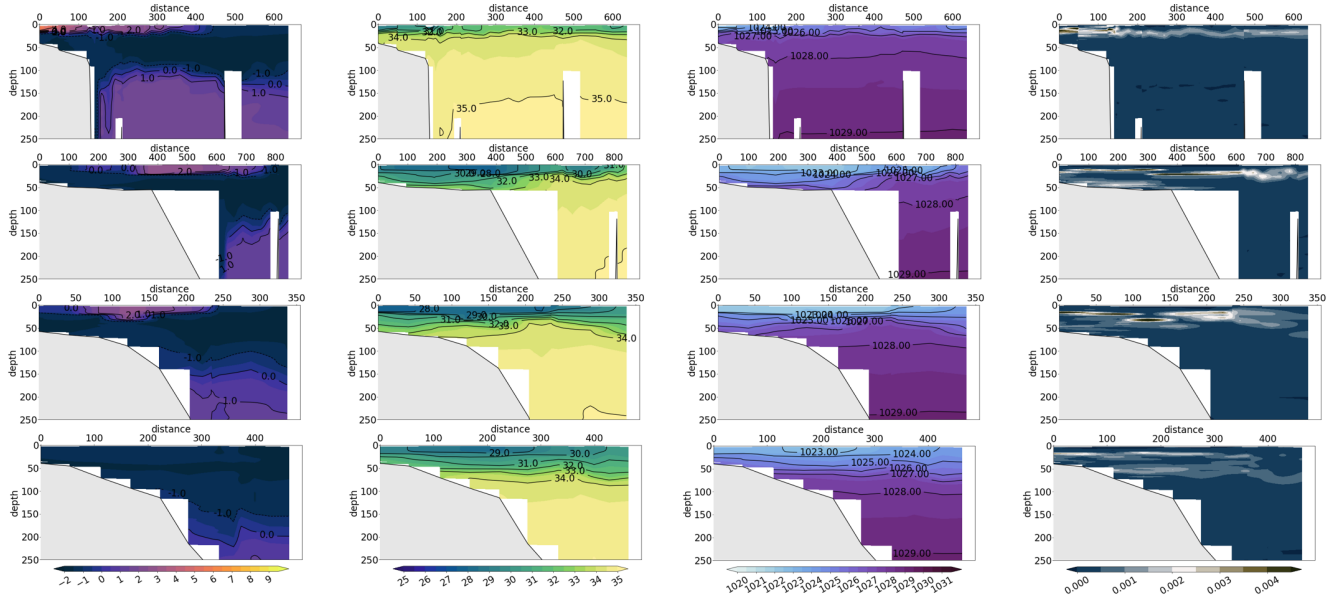

Figure 8. Conservative temperature (left, first column), absolute salinity (second column), density (third column) and Brünt-Vaisälä frequency (right, last column) in the upper 250 m along oceanographic section 5 (upper row); section 6 (second row); section 8 (third row); and section 7 (lower row). See Fig.1 for the section positions (the zero km is always placed at the southern point of each section)

4.1.2 Mean monthly observations.

In a previous study on this region (Dmitrenko et al. (2005)) claimed that the surface fronts displacement is mainly governed by the wind. To investigate it, we computed mean wind fields and the Ekman transport for August and September 2018 (Fig. 9). Horizontal transport was calculated as:

$$\begin{aligned} u_{ekm} &= \frac{\tau_v}{\rho_w * f} \\ v_{ekm} &= -\frac{\tau_u}{\rho_w * f} \end{aligned} \tag{1}$$

where u_{ekm} and v_{ekm} are horizontal components of the Ekman transport, τ is a wind stress, calculated from ASCAT winds (u_{wind}, v_{wind}) using ERA5 air density ρ_{air}: $\tau_u = C_D * (u_{wind}) * u_{wind} * \rho_{air}$; ρ_w is a surface density, calculated from SST and SSS with TEOS-2010; C_D is surface drag coefficient calculated from wind speed according to Foreman and Emeis (2010), f is the Coriolis parameter.

Vertical Ekman speed (upwelling and downwelling) was computed as:

$$w_{ekm} = \frac{1}{\rho_w * f}\left(\frac{d\tau_v}{dx} - \frac{d\tau_u}{dy}\right) + \frac{\beta * \tau_u}{\rho_w * f^2} \tag{2}$$

where w_{ekm} is a vertical component of the Ekman transport and β is the y-derivative of the Coriolis parameter.

https://doi.org/10.5194/os-2019-60
Preprint. Discussion started: 31 July 2019

The average wind speeds were low to moderate during two discussed summer months, 3-7 m/s. The wind field in August was more homogeneous and velocities slightly higher with general south-easterly direction; the Ekman transport pushed the river water out of the central part of the Laptev Sea favouring its propagation under the ice. A large area of convergence and downwelling is seen east of the Taimyr peninsula at 77°N 120°E. Almost the rest of the studied area is an upwelling zone, with large values of vertical velocity in the Vilkitskiy Strait and following the river front above the continental slope in the central part of the Laptev sea.

In September, the wind changed its main direction to the south-westerly, which led to river water blocking in the Yanskiy bay, still favouring the freshwater flux propagation under the ice, but mostly into southern part of the East-Siberian Sea. A large-scale divergence and upwelling in the north-west Laptev sea was observed as well. The Ekman vertical velocities in September differed from August. Several downwelling zones were observed: in front of the Lena delta, close to MIZ in the north-east, and in the deep part of the central Laptev sea. The irregular pattern of the upwelling and downwelling facilitate the mixing of different water masses, which is more active, thus, in September.

5 Observed water masses of the Laptev sea

To generalise our understanding of vertical structure of the studied area, we used the classical TS-analysis, first based on CTD measurements only. Fig. 10 shows the temperature-salinity distributions in the upper 200 m, where the color of marker indicates depth. The most prominent feature on the diagram is the transformed Atlantic water mass with salinity close to 34.5-35 PSS, temperatures from -0.5 to 2.5 °C lying at a depth of 100-200 m. The water mass overlying the Atlantic water (between 50 and 100 m depth) is the lower halocline water, described by Dmitrenko et al. (2012) as having salinity in a range 33-34.5 PSS, and negative temperatures starting from the lowest values presented in Fig. 10, -1.7 to 2.5°C. The surface water observed in the upper 50 metres is in general the less saline (below 34 PSS), but one can clearly observe two separate branches with negative and positive temperatures. It should be remembered that TS-diagram based only on CTD measurements does not provide an instantaneous view on the ocean state, but is a collection of sea states in different regions at different moments of time (from the end of August to the end of September 2018). During summer months, the Arctic ocean waters quickly change their characteristics, and satellite data provide additional information to the pointwise in situ measurements.

Using DMI SST and SMOS SSS weekly estimates, we plotted T-S diagrams similar to that on in Fig.10, but for several reference days: Aug 1, Aug 15, Aug 30, Sept 4, Sept 13, and Sept 30, 2018 (Fig.11). On the lower row, we present all in situ measurements in the upper 6.5 m and the differences between satellite derived temperature and salinity of discussed days. It is clearly seen that the SST is rising only up to the end of August with the maximum temperatures from 8 to 11.5$^{\circ}C$ for some case, and then decreases to 4.5 $^{\circ}C$ by the end of September. The temperature is changing by 0.5 - 1 degree per week (while increasing and decreasing).

Based on the Fig. 11 visual analysis, we propose to identify 6 surface water masses in the Laptev and East-Siberian seas (Tab.1). The "classical" water masses are warm and fresh river waters ("1") and cold and saline open sea waters ("6"). All other water masses shows different stages of transformation of these two or water masses advected from other regions. It should be

https://doi.org/10.5194/os-2019-60
Preprint. Discussion started: 31 July 2019

Ocean Science
Discussions
Open Access
EGU

Table 1. Surface water masses

Water mass	1	2	3	4	5	6
T	$> 3°C$	$> 3°C$	$< 3°C$	$< 3°C$	$> 3°C$	$< 3°C$
S	$< 25PSS$	$25 - 29PSS$	$< 25PSS$	$25 - 29PSS$	$> 29PSS$	$> 29PSS$

noted that satellite-derived data have a larger range than surface in situ measurements, which makes this detailed classification possible. Positions of defined water masses for selected days are shown in Fig.12 together with the distribution of water masses in percentage (the whole studied area is 100% and sea ice occupies some part).

On August 1, the sea ice still covers more than 80% of the studied area and extends on average to 78°N in the Laptev sea, while the East-Siberian Sea is covered almost completely. Warm and fresh river water ("1") is well observable in the south between 74 and 76°N. It occupies almost the same amount of surface as cold and saline sea water ("6"), the rest of the open area is a transformed river water (”2”, ”4”), that forms already a recognisable river front: its signature is continuous from 115°E to 150°E up to the northern position of sea edge.

In two weeks the ice cover retreats, and a fresh and cold water ("3") mass appears in the south-west East-Siberian sea. The amount of this waters increases progressively in this area during the remaining period. We suggest that this water mass represents the river waters captured under the ice and then exposed back.

On the 15th of August, one can notice as well a water mass "4" appearing close to Vilkitskiy Strait. It is less pronounced in the end of August, but a thin stream of cooled and transformed river waters from the Kara sea descends along the Taimyr peninsula in September. The Lena river waters mixing and cooling happens as well close to the sea ice edge in the north-east Kara sea. All in all, the surface occupied by this water mass is steadily growing during the observed period, and is around 10% by the end of September. One can imagine that water mass "4" is a transformed version of water mass "3".

The end of August is warmest, it is seen in Fig. 12 with the amount of saline waters with temperatures above $3°C$ (water mass "5") occupying the central and the western part of the Laptev sea (almost 10% of the studied area). This water mass is disappearing by the end of September with a decrease of temperature.

By September 13, the SST and SSS variability slow down. The water mass "3" in the north-east Laptev sea consisting of cold fresh water becomes saltier (transforms into the water mass "4"). The fresh water cools south of the New Siberian island and by September 25 occupies all the area free of ice. The river plumes signature is shifted to the New Siberian island as well (Fig. 12). Saline and cold water mainly dominates the surface of the Laptev Sea. Finally, by September 25, the T-S diagram shows that most of the points lay between 25 and 35 PSS and -1°C and 4°C, with a main core within a range 25-35 PSS and -1 to 1°C. The Laptev and the East-Siberian seas start to refreeze, most rapidly in the area with cold and fresh river waters.

https://doi.org/10.5194/os-2019-60
Preprint. Discussion started: 31 July 2019

6 Discussion and conclusion

In this work, we discussed the water masses evolution in the summertime in the Laptev and the East-Siberian seas. The cross-validation of satellite-derived SST L4 distributed by DMI was done with continuous TSG measurements. For the first time the capacity of SMOS to follow a temporal evolution of the Lena river plume in the Laptev sea under influence of atmospheric forcing was demonstrated.

A pathway of the low salinity Kara waters was observed during several days of the studied period. Kara waters propagated mostly through the Vilkitskiy Strait and partly through the Shokalskiy Strait, but no freshwater was found northward of the Severnaya Zemlya Archipelago. Pursuing the coastline, this low salinity water arrives into the Oleneksiy bay where it meets another freshwater flux from the Lena and Khatanga rivers.

The wind situation in August was favorable for the extreme propagation of river waters into the central and the north-eastern part of the Laptev sea with following penetration into the East-Siberian sea in MIZ and under the sea ice. The fresh waters displacement was associated with the Ekman transport. We claim as well that a similar propagation of river waters far to the North happened before the observed period (in June-July), when the Laptev sea was still covered with ice and the Lena river discharge was supposed to be the maximum (following the results of Papa et al. (2008)). In the north of the 126°E section, under the ice, the upper 25-m layer is fresher with a salinity below 33 PSS, which supports this hypothesis; and there is no evidence that the sea ice melting itself can create such a considerable layer of freshwater. A study of Bauch and Cherniavskaia (2018) defend the hypothesis of river waters, as similar situation was observed in 2011. Unfortunately, the present spatial resolution of satellite-derived SSS and its uncertainty due to the ice proximity make difficult to separate river waters from the freshening associated with the sea ice melting. No direct measurements of sea ice thickness were carried out in this region at this time, so it is complicated to evaluate the freshwater input due to the sea ice melting only. The propagation of river waters under the sea ice is apparent in the western part of the East-Siberian sea, where two brunches with warm and fresh cores were observed with in situ data.

In September, we illustrated the processes of rapid autumn cooling of the surface waters in the Laptev sea associated with a series of atmospheric depressions. Calculated monthly Ekman pumping indicates the area of most intense mixing processes. A new sea level dataset provided by DTU for the Arctic ocean and calculated geostrophic currents, discussed in the Appendix, enriches the overview of the surface ocean dynamics during selected summer months.

To generalise the evolution of surface water masses, a variation of a classical TS analysis was proposed using satellite measurements. It helped to define new surface water masses adapted for the Arctic ocean with typically low salinity. As the validity of SMOS SSS was demonstrated successfully and SMOS measurements are accessible from 2010 to the present moment, this technique can be applied for further interannual analysis of surface water transformation.

Appendix A: Altimetry and geostrophic currents

Two monthly fields of absolute dynamic topography (ADT) and geostrophic currents were calculated from sea level anomalies (SLA) Arctic L4 product and mean dynamic topography (MDT) provided by Danish technological University (Fig. A1).

https://doi.org/10.5194/os-2019-60
Preprint. Discussion started: 31 July 2019

Sea level anomalies are available as mean monthly values on a grid adapted to polar regions with 0.25°step for latitudes, and 0.5°step for longitudes. Mean dynamic topography global one-minute model was used to compute ADT. The resulting monthly absolute dynamic topography ($ADT = MDT + SLA$) was calculated for selected summer months. Overall, the ADT follows remarkably the ocean bottom topography with higher SLA over the shelf and lower SLA over the deep part of the studied area. The only exception is negative SLA in the Olenekskiy bay in August 2018. We suggest that the general northward wind-induced displacement of the waters over the very shallow southern part of the sea was compensated only by the river waters inflow to the east of 122°E, close to the Lena river delta. Positive SLA were more pronounced in September than in August, though in August the SST was higher over the southern and central part of the Laptev sea, and the salinity was lower in the Olenekskiy bay. The importance of sterical component in variation of the sea level in August-September is thus doubtful, though several source of uncertainty can impact the quality of provided SLA data: uncertainty in tidal model, bathymetry precision, accuracy of the MDT over the shallow part of the Laptev sea, etc.

The geostrophic currents were calculated following classical formula: $u_g = \frac{-g}{f}\frac{dh}{dy}$, $v_g = \frac{g}{f}\frac{dh}{dx}$, where h is ADT, x and y are the distance in metres. Geostrophic currents presented in Fig.A1 are very weak and demonstrate rather chaotic structures during selected months. Among the well-pronounced features, an outflow from the Laptev sea in the Vilkitskiy strait is noticeable. Above the continental slope edge, the principal direction of currents is the westward with a maximum current speed of 0.5 m/s. In the south, an outflow at 122 °E and 130°E helps to bring the Lena waters into the central part of the Laptev sea. In the Yanskiy bay a vortex-like system exists in both August and September 2018. Geostrophic currents in the East-Siberian sea were calculated from the altimetric measurements in MIZ, so should be interpreted with care. A cyclonic feature of 150 km in diameter is seen at 79°N, 157°E, and might be topographically induced, as well as a similar cyclonic feature at 78.5°N 135°E. An extended study should be carried out to validate the accuracy of altimetry-derived currents in this region with mooring or vessel mounted ADCP measurements.

Competing interests. No competing interests are present

Acknowledgements. We thank Jean-Luc Vergely for fruitful discussions about SMOS SSS data filtering in the Arctic ocean. This study was supported by the French CNES-TOSCA SMOS-OCEAN project. Anastasiia Tarasenko, Vladimir Ivanov and Nikita Kusse-Tiuz acknowledges financial support from the Ministry of Science and Higher Education of the Russian Federation, project RFMEFI61617X0076.

https://doi.org/10.5194/os-2019-60
Preprint. Discussion started: 31 July 2019

References

Aagaard, K. and Carmack, E. C.: The role of sea ice and other fresh water in the Arctic circulation, Journal of Geophysical Research: Oceans, 94, 14 485–14 498, 1989.

Amante, C. and Eakins, B. W.: ETOPO1 arc-minute global relief model: procedures, data sources and analysis, 2009.

Andersen, O. B. and Johannessen, J. A.: The High Latitude Seas and Arctic Ocean, in: Satellite Altimetry Over Oceans and Land Surfaces, pp. 271–296, CRC Press, 2017.

Arias, M. and Laboratories, S.-O. E. S.: L2OS v662 Reprocessing Report, SO-RP-ARG-GS-0109., available on https://smos.argans.co.uk/docs/reports/SO-RP-ARG-GS-0109$_L2OS_Reprocessing_Report_v2.6_170717.pdf.$, 2017.

Bauch, D. and Cherniavskaia, E.: Water mass classification on a highly variable arctic shelf region: Origin of laptev sea water masses and implications for the nutrient budget, Journal of Geophysical Research: Oceans, 123, 1896–1906, 2018.

Bertino, L., Lisæter, K., and Scient, S.: The TOPAZ monitoring and prediction system for the Atlantic and Arctic Oceans, Journal of operational oceanography, 1, 15–18, 2008.

Boutin, J., Vergely, J.-L., Marchand, S., d'Amico, F., Hasson, A., Kolodziejczyk, N., Reul, N., Reverdin, G., and Vialard, J.: New SMOS Sea Surface Salinity with reduced systematic errors and improved variability, Remote Sensing of Environment, 214, 115–134, 2018.

Castro, S. L., Emery, W. J., Wick, G. A., and Tandy, W.: Submesoscale Sea Surface Temperature Variability from UAV and Satellite Measurements, Remote Sensing, 9, 1089, 2017.

Cherniavskaia, E. A., Sudakov, I., Golden, K. M., Strong, C., and Timokhov, L. A.: Observed winter salinity fields in the surface layer of the Arctic Ocean and statistical approaches to predicting large-scale anomalies and patterns, Annals of Glaciology, 59, 83–100, 2018.

de Boyer Montégut, C., Madec, G., Fischer, A. S., Lazar, A., and Iudicone, D.: Mixed layer depth over the global ocean: An examination of profile data and a profile-based climatology, Journal of Geophysical Research: Oceans, 109, 2004.

Dinnat, E. P., M. Le Vine, D., Boutin, J., Meissner, T., and Lagerloef, G.: Remote Sensing of Sea Surface Salinity: Comparison of Satellite and In Situ Observations and Impact of Retrieval Parameters, Remote Sensing, 11, 2019.

Dmitrenko, I., Kirillov, S., Eicken, H., and Markova, N.: Wind-driven summer surface hydrography of the eastern Siberian shelf, Geophysical Research Letters, 32, 2005.

Dmitrenko, I. A., Kirillov, S. A., Ivanov, V. V., Rudels, B., Serra, N., and Koldunov, N. V.: Modified halocline water over the Laptev Sea continental margin: Historical data analysis, Journal of Climate, 25, 5556–5565, 2012.

Foreman, R. J. and Emeis, S.: Revisiting the definition of the drag coefficient in the marine atmospheric boundary layer, Journal of Physical Oceanography, 40, 2325–2332, 2010.

Grodsky, S., Vandemark, D., and Feng, H.: Assessing Coastal SMAP Surface Salinity Accuracy and Its Application to Monitoring Gulf of Maine Circulation Dynamics, Remote Sensing, 10, 1232, 2018.

Haine, T. W., Curry, B., Gerdes, R., Hansen, E., Karcher, M., Lee, C., Rudels, B., Spreen, G., de Steur, L., Stewart, K. D., et al.: Arctic freshwater export: Status, mechanisms, and prospects, Global and Planetary Change, 125, 13–35, 2015.

Høyer, J. L., Le Borgne, P., and Eastwood, S.: A bias correction method for Arctic satellite sea surface temperature observations, Remote Sensing of Environment, 146, 201–213, 2014.

Ivanov, V., Varentsov, M., Matveeva, T., Repina, I., Artamonov, A., and Khavina, E.: Arctic Sea Ice Decline in the 2010s: The Increasing Role of the Ocean—Air Heat Exchange in the Late Summer, Atmosphere, 10, 184, 2019.

https://doi.org/10.5194/os-2019-60
Preprint. Discussion started: 31 July 2019

Janout, M. A., Hölemann, J., Timokhov, L., Gutjahr, O., and Heinemann, G.: Circulation in the northwest L aptev S ea in the eastern A rctic O cean: Crossroads between S iberian R iver water, A tlantic water and polynya-formed dense water, Journal of Geophysical Research: Oceans, 122, 6630–6647, 2017.

Klein, L. and Swift, C.: An improved model for the dielectric constant of sea water at microwave frequencies, IEEE Journal of Oceanic Engineering, 2, 104–111, https://doi.org/10.1109/JOE.1977.1145319, 1977.

Olmedo, E., Gabarró, C., González-Gambau, V., Martínez, J., Ballabrera-Poy, J., Turiel, A., Portabella, M., Fournier, S., and Lee, T.: Seven Years of SMOS Sea Surface Salinity at High Latitudes: Variability in Arctic and Sub-Arctic Regions, Remote Sensing, 10, 1772, 2018.

Papa, F., Prigent, C., and Rossow, W. B.: Monitoring flood and discharge variations in the large Siberian rivers from a multi-satellite technique, Surveys in Geophysics, 29, 297–317, 2008.

Pfirman, S., Bauch, D., and Gammelsrød, T.: The northern Barents Sea: water mass distribution and modification, AGU, Ameircan Geophysical Union, 1994.

Pnyushkov, A. V., Polyakov, I. V., Ivanov, V. V., Aksenov, Y., Coward, A. C., Janout, M., and Rabe, B.: Structure and variability of the boundary current in the Eurasian Basin of the Arctic Ocean, Deep Sea Research Part I: Oceanographic Research Papers, 101, 80–97, 2015.

Polyakov, I. V., Alexeev, V., Belchansky, G., Dmitrenko, I. A., Ivanov, V., Kirillov, S. A., Korablev, A., Steele, M., Timokhov, L. A., and Yashayaev, I.: Arctic Ocean freshwater changes over the past 100 years and their causes, Journal of Climate, 21, 364–384, 2008.

Rabe, B., Karcher, M., Schauer, U., Toole, J. M., Krishfield, R. A., Pisarev, S., Kauker, F., Gerdes, R., and Kikuchi, T.: An assessment of Arctic Ocean freshwater content changes from the 1990s to the 2006–2008 period, Deep Sea Research Part I: Oceanographic Research Papers, 58, 173–185, 2011.

Rudels, B., Jones, E. P., Schauer, U., and Eriksson, P.: Atlantic sources of the Arctic Ocean surface and halocline waters, Polar Research, 23, 181–208, 2004.

Spreen, G., Kaleschke, L., and Heygster, G.: Sea ice remote sensing using AMSR-E 89-GHz channels, Journal of Geophysical Research: Oceans, 113, 2008.

Tang, W., Yueh, S., Yang, D., Fore, A., Hayashi, A., Lee, T., Fournier, S., and Holt, B.: The Potential and Challenges of Using Soil Moisture Active Passive (SMAP) Sea Surface Salinity to Monitor Arctic Ocean Freshwater Changes, Remote Sensing, 10, 869, 2018.

Timmermans, M.-L., Cole, S., and Toole, J.: Horizontal density structure and restratification of the Arctic Ocean surface layer, Journal of Physical Oceanography, 42, 659–668, 2012.

Timokhov, L. A. and Chernyavskaya, E. A.: Osobennosti sostoyaniya poverhnostnogo sloya arkticheskogo basseina v anomal'noe leto 2007, Arctic and Antarctic Problems, pp. 19–27, 2009.

Tryoshnikov, A.: Osnovnye zadachi i itogi natsional'nogo naturnogo experimenta «POLEX-Sever-76», Leningrad Gidrometeoizdat, 1979.

Vivier, F., Hutchings, J. K., Kawaguchi, Y., Kikuchi, T., Morison, J. H., Lourenço, A., and Noguchi, T.: Sea ice melt onset associated with lead opening during the spring/summer transition near the North Pole, Journal of Geophysical Research: Oceans, 121, 2499–2522, 2016.

Yin, X., Boutin, J., and Spurgeon, P.: Biases Between Measured and Simulated SMOS Brightness Temperatures Over Ocean: Influence of Sun, IEEE Journal of Selected Topics in Applied Earth Observations and Remote Sensing, 6, 1341–1350, https://doi.org/10.1109/JSTARS.2013.2252602, 2013.

https://doi.org/10.5194/os-2019-60
Preprint. Discussion started: 31 July 2019

Ocean Science
Discussions
Open Access
EGU

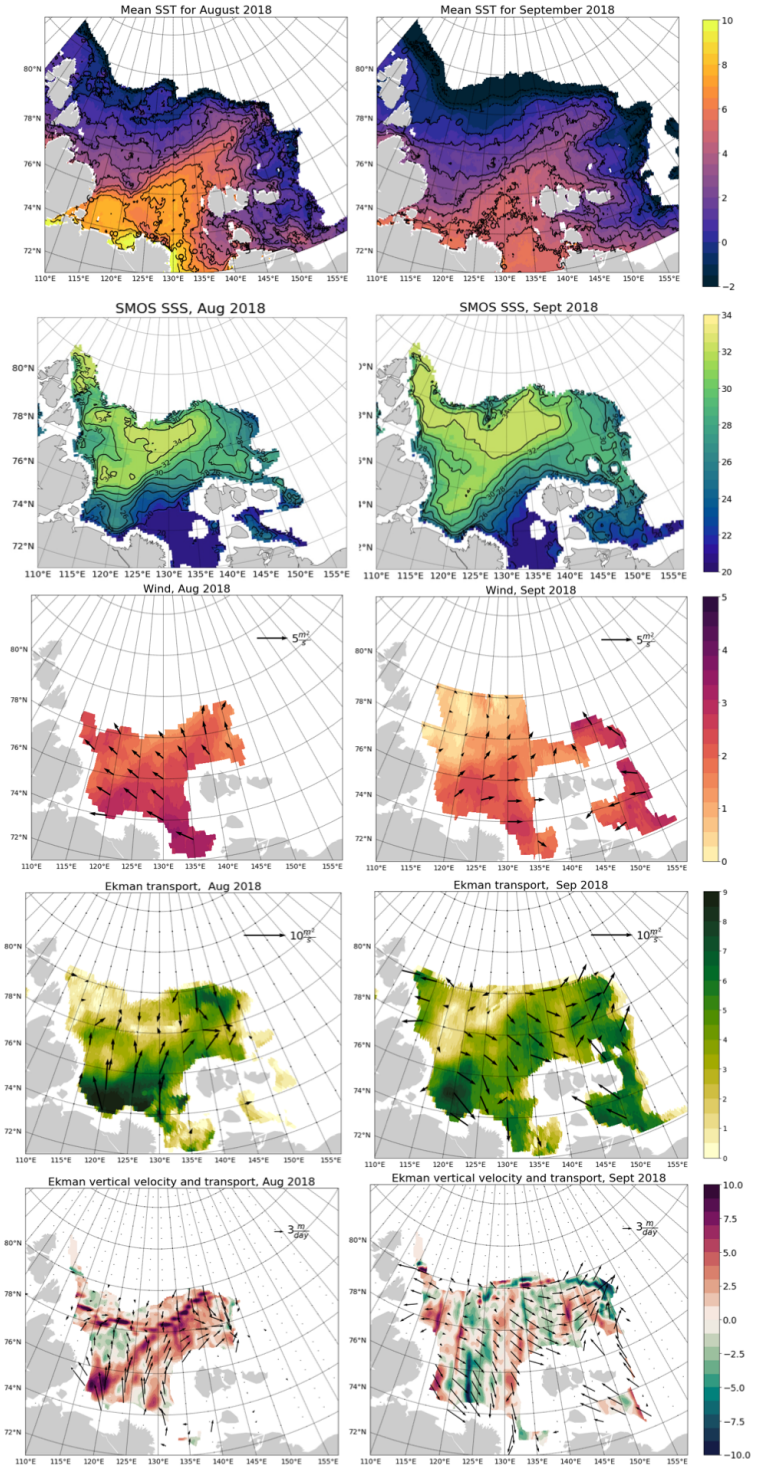

Figure 9. Mean monthly averages for August (upper row) and September (lower row): (a) SST, (b) SSS, (c) wind speed and direction; (d-e) horizontal and vertical Ekman transport

https://doi.org/10.5194/os-2019-60
Preprint. Discussion started: 31 July 2019

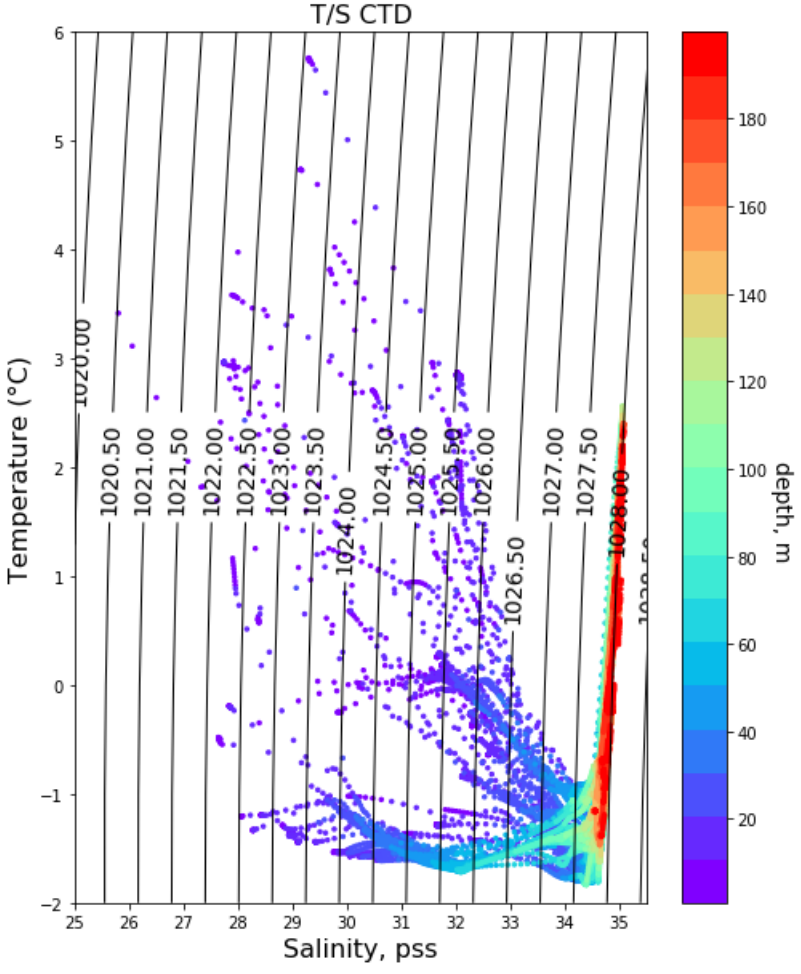

Figure 10. TS diagram based on the CTD data in the upper 200 m

https://doi.org/10.5194/os-2019-60
Preprint. Discussion started: 31 July 2019

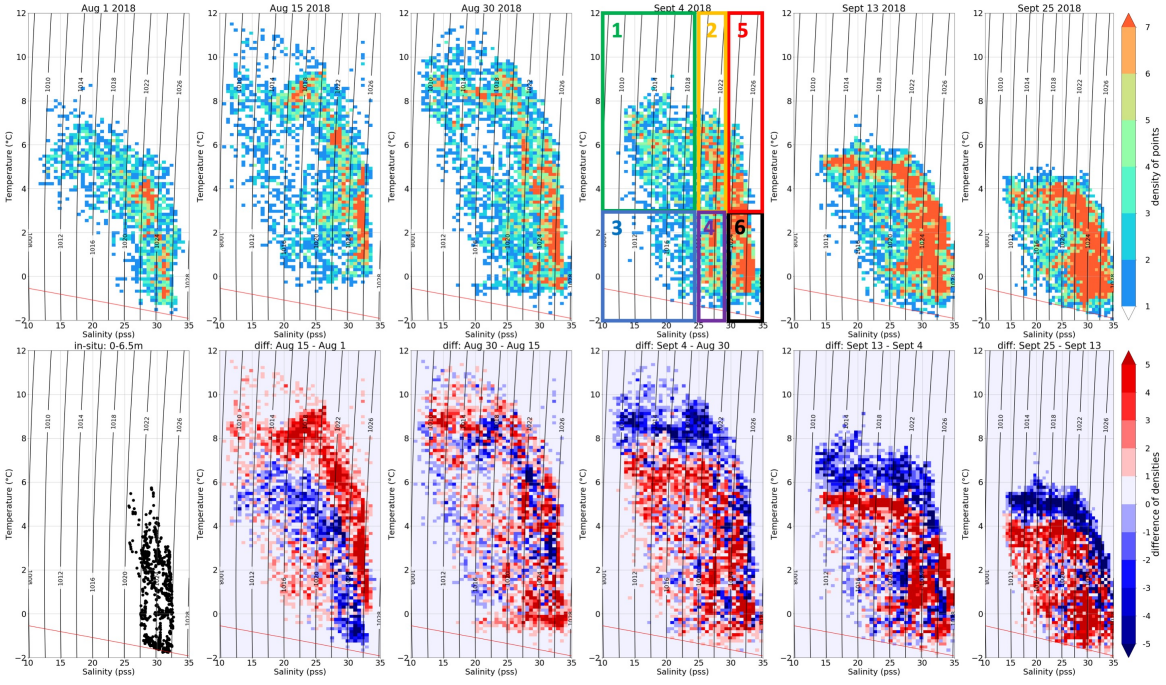

Figure 11. Temporal evolution of surface water masses in August-September 2018 for the following reference days (upper row): Aug 1, Aug 15, Aug 30, Sept 4, Sept 13, and Sept 30, 2018. Color represents the density of points (number of observations with this temperature and salinity). Lower row: T-S diagram based on CTD measurements in the upper 6.5 m only, and the differences (in density points) between the reference days.

https://doi.org/10.5194/os-2019-60
Preprint. Discussion started: 31 July 2019

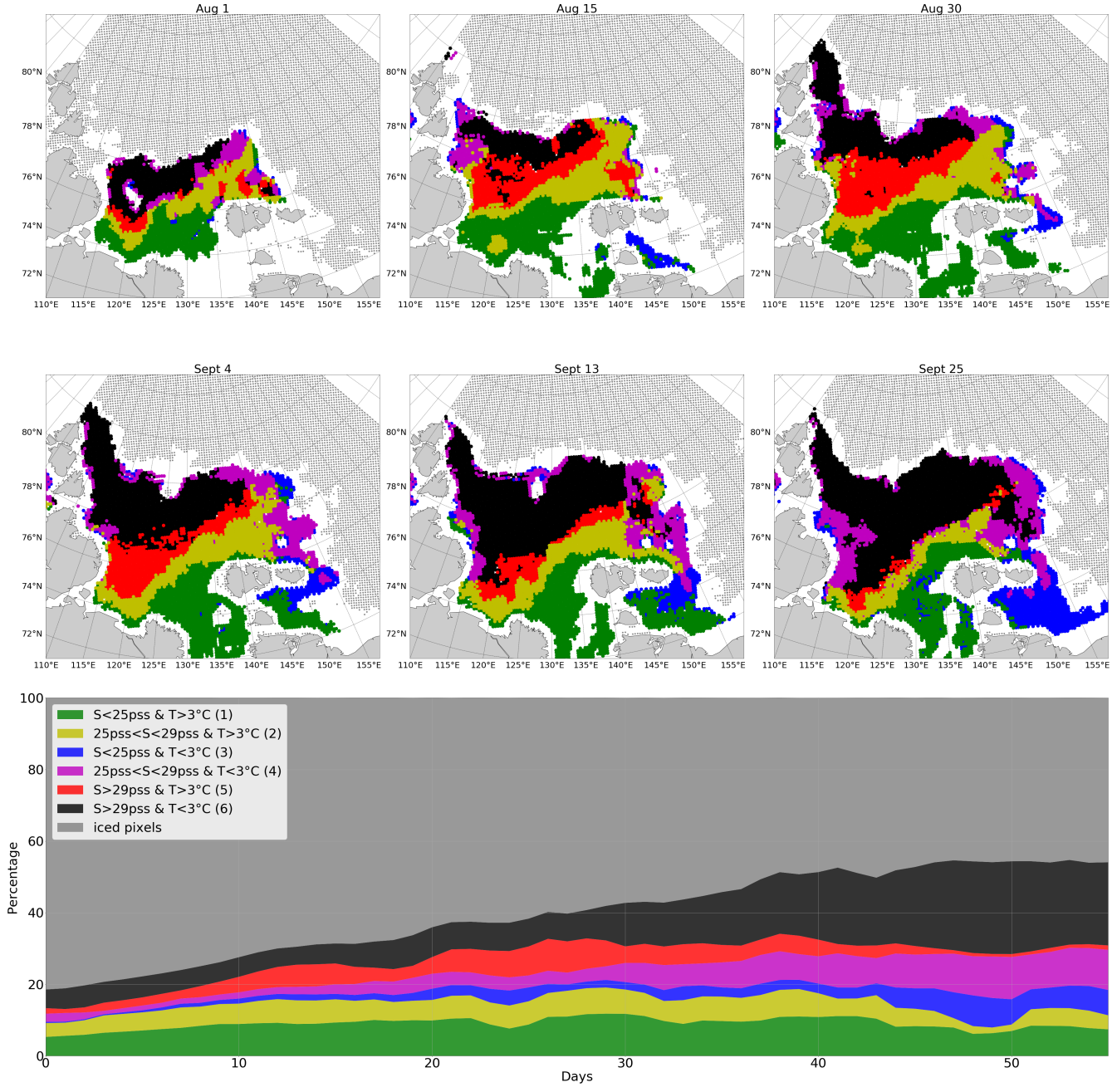

Figure 12. Water masses spatial distribution in August-September 2018: upper row - Aug 1, Aug 15, Aug 30; lower row - Sept 4, Sept 13, Sept 30. Sea ice cover from AMSR2 is plotted as dashed area.

https://doi.org/10.5194/os-2019-60
Preprint. Discussion started: 31 July 2019

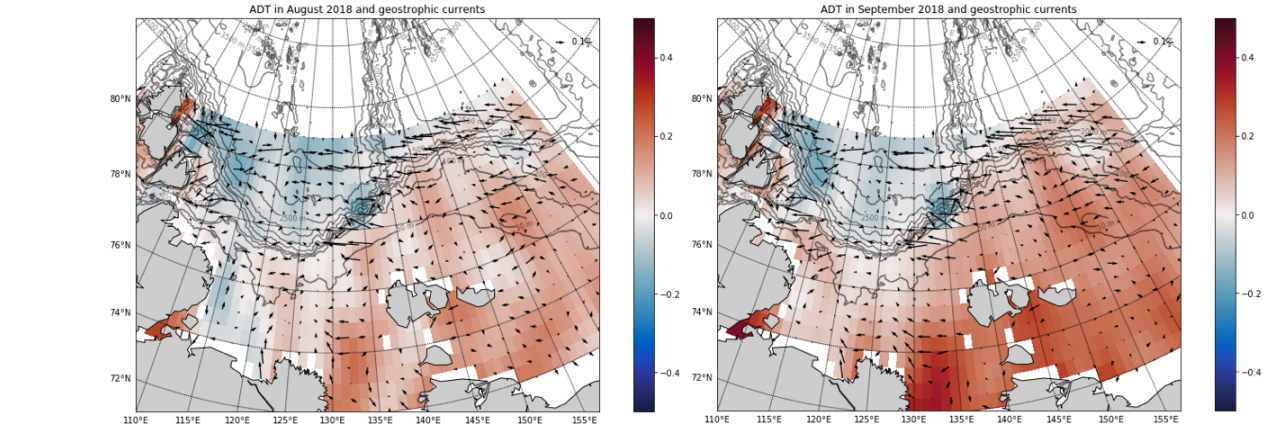

Figure A1. Absolute dynamic topography and geostrophic currents in August and September 2018, calculated from DTU monthly Sea Level anomaly